GFZ
Helmholtz-Zentrum
POTSDAM

Originally published as:

Deal, E., Favre, A.-C., Braun, J. (2017): Rainfall variability in the Himalayan orogen and its relevance to erosion processes. - *Water Resources Research*, *53*, 5, pp. 4004—4021.

DOI: http://doi.org/10.1002/2016WR020030

AGU PUBLICATIONS

Water Resources Research

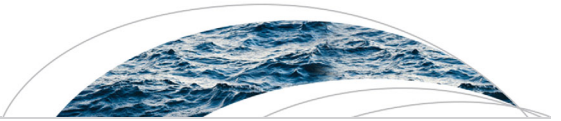

RESEARCH ARTICLE
10.1002/2016WR020030

Rainfall variability in the Himalayan orogen and its relevance to erosion processes

Eric Deal[1,2], Anne-Catherine Favre[3], and Jean Braun[1,2]

[1]ISTerre, Université Grenoble Alpes, Grenoble, France, [2]Helmholtz Centre Potsdam, German Research Center for Geosciences (GFZ), Telegrafenberg, Potsdam, Germany, [3]LTHE, GINP/ENSE3, Université Grenoble Alpes, Grenoble, France

Key Points:
- Characterization of distribution of daily rainfall, revealing large-scale patterns in daily rainfall variability
- Quantification of negative correlation between rainfall mean and rainfall variability
- Discussion of the influence of rainfall variability on short and long-term erosion rates

Correspondence to:
E. Deal,
edeal@gfz-potsdam.de

Citation:
Deal, E., A.-C. Favre, and J. Braun (2017), Rainfall variability in the Himalayan orogen and its relevance to erosion processes, *Water Resour. Res.*, *53*, 4004–4021, doi:10.1002/2016WR020030.

Received 3 NOV 2016
Accepted 20 APR 2017
Accepted article online 26 APR 2017
Published online 16 MAY 2017

Abstract Rainfall is an important driver of erosion processes. The mean rainfall rate is often used to account for the erosive impact of a particular climate. However, for some erosion processes, erosion rate is a nonlinear function of rainfall, e.g., due to a threshold for erosion. When this is the case, it is important to take into account the full distribution of rainfall, instead of just the mean. In light of this, we have characterized the variability of daily rainfall over the Himalayan orogen using high spatial and temporal resolution rainfall data sets. We find significant variations in rainfall variability over the Himalayan orogen, with increasing rainfall variability to the west and north of the orogen. By taking into account variability of rainfall in addition to mean rainfall rate, we find a pattern of rainfall that, from a geomorphological perspective, is significantly different from mean rainfall rate alone. Using these findings, we argue that short-term rainfall variability may help explain observed short and long-term erosion rates in the Himalayan orogen.

Plain Language Summary An important topic in earth science is understanding how climate and tectonic forces interact to shape the surface of the Earth. One of the main influences that climate has on the Earth's surface is to cause erosion by delivering water to landscapes as rain and snow. Wetter climates should, in general, cause more erosion than drier climates, which is why the mean annual rainfall has traditionally been used as a measure of the erosive strength of climate. However, field evidence seems to suggest that the effect of climate is more sophisticated than can be captured with the mean annual rainfall. There is a considerable body of theory demonstrating that the intensity of rainfall, or storminess, is an equally important aspect of how climate causes erosion. In light of this, we have characterized the storminess in the Himalayan mountain range, a place with high erosion rates driven by rainfall. We show that there is large variation in storminess from place to place in the Himalayas, and that this can help explain observed rates of erosion, which do not match mean annual rainfall rates.

1. Introduction

The discrete and episodic nature of erosion events can often be attributed to the intermittent, variable nature of rainfall, one of the principle drivers of erosion. Rainfall plays a vital role in shaping landscapes; many erosion processes require or are accelerated by the presence of water. It is for this reason that many studies attempting to untangle the relationship between climate and erosion compare measured erosion rates to mean rainfall rates and a derivative of it, specific stream power (a surrogate for fluvial erosion which is a function of rainfall rate, slope steepness, and channel width) [e.g., *Burbank et al.*, 2003; *Dadson et al.*, 2003; *Craddock et al.*, 2007; *Burbank et al.*, 2012; *Adlakha et al.*, 2013; *Scherler et al.*, 2014; *Hirschmiller et al.*, 2014; *Godard et al.*, 2014]. Implicit in this comparison is the assumption that the details of rainfall, such as storm size and frequency, are unimportant, that more water yields more erosion. However, this only makes sense if the instantaneous (single event timescale) erosion rate scales linearly with the instantaneous rainfall rate. If the instantaneous erosion rate is instead a nonlinear function of the instantaneous rainfall rate or there are thresholds below which no erosion takes place, the relationship between long-term water availability and erosion will be more complicated. Thresholds have been demonstrated or hypothesized in many erosion processes including overland flow on vegetated slopes [*Horton*, 1945], channel initiation [e.g., *Dietrich et al.*, 1993; *Prosser and Dietrich*, 1995; *Tucker and Slingerland*, 1997], sediment entrainment in rivers

© 2017. The Authors.
This is an open access article under the terms of the Creative Commons Attribution-NonCommercial-NoDerivs License, which permits use and distribution in any medium, provided the original work is properly cited, the use is non-commercial and no modifications or adaptations are made.

[e.g., *Wolman and Miller*, 1960; *Andermann et al*., 2012], landsliding and mass wasting [e.g., *Gabet et al*., 2004], and fluvial erosion of gravel bed and bedrock rivers [e.g., *Tucker and Bras*, 2000; *Lague*, 2005; *Beer and Turowski*, 2015]. Nonlinearities have also been proposed [e.g., *Lague*, 2005], though it can be difficult to distinguish a nonlinearity from a threshold [*DiBiase et al*., 2010].

Erosion thresholds or nonlinear dependence on the instantaneous rainfall rate make it necessary to have information about the magnitude and frequency of individual storms. A common surrogate for single storms is the daily rainfall rate, because it is a natural timescale that is similar to the duration of individual storms and reflects the frequency of many rainfall time series. Previous work has shown theoretically that in the presence of erosion thresholds or nonlinear dependence on rainfall, long-term erosion rates will be sensitive to the variability of daily rainfall [e.g., *Tucker and Bras*, 2000; *Tucker*, 2004; *Lague*, 2005] with some evidence to support this claim [*Snyder et al*., 2003; *DiBiase et al*., 2010]. The general conclusion is that higher variability will drive higher erosion rates. Although this work is with reference to erosion by bedrock rivers, the same concepts apply to any erosion process with nonlinearities or thresholds that is driven by a highly variable forcing such as rainfall.

If daily rainfall variability is a feature of rainfall that, in addition to the mean rainfall rate, modulates the impact of rainfall on erosion rates, then it may help to explain the inconsistency between modern climate and erosion rates in the Himalayan orogen. In the orogen interior, erosion rates inferred from thermochronological data increase across a topographic divide towards the Tibetan plateau despite decreasing mean rainfall rates [*Burbank et al*., 2003; *Thiede and Ehlers*, 2013]. Here the topographic divide is defined as the average location of the major peaks in the orogen that form the southern edge of the Tibetan plateau. It is this east west trending range of high peaks that creates a rain shadow to the north, and can be associated with both the northwards increasing erosion rates and decreasing rainfall rates. Here we characterize the daily variability of rainfall in the Himalayan orogen, and discuss the spatial patterns found, as well as the implications for erosion processes driven by rainfall.

There are several established methods for characterizing the daily variability of rainfall. Extreme rainfall analyses describe the most intense days of rainfall, their frequency of occurrence, and magnitude. This has obvious value to human society, and has been applied to the Himalayan orogen [e.g., *Bharti et al*., 2016; *Joshi et al*., 2014], where intense monsoon storms can cause significant economic damage [*Thayyen et al*., 2013]. Here, we are not attempting an extreme value assessment of daily rainfall. Theoretical work accounting for erosion thresholds and nonlinearities argues that it is not just extreme events that are potentially significant, but also the distribution of moderate magnitude events (e.g., annual maximum storm or even smaller, depending on the erosion threshold) [*Wolman and Miller*, 1960; *Tucker and Bras*, 2000; *Tucker*, 2004; *Snyder et al*., 2003; *Lague*, 2005, 2014]. Also, we do not wish to estimate future rainfall statistics, but rather to characterize the observed distribution of daily rainfall, and do so as succinctly as possible. Characterizing variability by fitting a function to some empirical form of the distribution of daily rainfall is another established technique. Whether the function is fit to the empirical frequency distribution [e.g., *May*, 2004a; *Suhaila et al*., 2011], the normalized rainfall curve [e.g., *Burgueño et al*., 2010], or the concentration index [e.g., *Martin-Vide*, 2004; *Jiang et al*., 2016; *Caloiero*, 2014] the result is the same: the actual form of the distribution of daily rainfall variability is summarized by a function with just a few parameters. In order to keep in line with previous work on the importance of climatic variability on long-term landscape evolution [*Tucker and Bras*, 2000; *Tucker*, 2004; *Lague*, 2005; *Rossi et al*., 2016], we fit a mixture of gamma distributions to the empirical frequency distribution of daily rainfall.

In this study, we make use of two high spatial and temporal resolution gridded rainfall data sets. Several studies have characterized the daily variability of rainfall using high spatial resolution gridded data sets [e.g., *Burgueño et al*., 2010; *Jiang et al*., 2016], however, not over the Himalayan orogen. Several others describe the distribution of Indian rainfall using similar methods to those employed in this study [*Mooley*, 1973; *May*, 2004a,b]. However, they make use of data sets with low spatial resolution and tend to focus on rainfall patterns across the Indian subcontinent rather than the orogen. *Prakash et al*. [2015b] compute the coefficient of variation of monsoon rainfall, which is closely related to daily variability, using TMPA and other high-resolution gridded data sets, however by restricting the analysis to India, they leave out much of the Himalayan orogen. Finally, there are several studies comparing the frequency-magnitude distribution of daily rainfall to erosion patterns in the Himalayas [e.g., *Bookhagen and Burbank*, 2010; *Craddock et al*., 2007; *Wulf et al*., 2010, 2012]. However, these studies do so only from the perspective of extreme events and often

only on the scale of single valleys. The previous studies of daily variability of Indian and Himalayan rainfall are useful to corroborate our results where the different data sets overlap. However, they do not allow for a careful assessment of daily variability over the entire Himalayan orogen, which is the goal of this study.

2. Data and Methods

2.1. Data

In recent years, several rainfall data sets spanning the entire Himalayan orogen have become available, ranging from moderate to high temporal and spatial resolution. We use two, described below, that are known to perform well in the Himalayan orogen [*Andermann et al*., 2011].

2.1.1. APHRODITE

Asian rainfall Highly Resolved Observational Data Integration Towards Evaluation of Water Resources, Monsoon Asia, Version 11—APHRO_MA_025deg_V1101R2 (referred to here as APHRODITE) is a distance-weighted interpolation of daily rainfall depths from between 5000 and 12,000 ground-based stations (depending on the time period) spread throughout Asia over the period from 1951 to 2007. It is made available by the Research Institute for Humanity and Nature (RIHN) Japan and the Meteorological Research Institute of Japan Meteorological Agency (MRI/JMA). The data set has a spatial resolution of $0.25^\circ \times 0.25^\circ$, and a temporal resolution of 1 day [*Yatagai et al*., 2012]. Despite making use of an orographic correction algorithm, there are concerns with the accuracy of the data set due to the relatively small number of stations it is interpolated from in the orogen. Particularly outside of Nepal and north of the main topographic divide. *Andermann et al*. [2011] tested the accuracy of this data set in the Himalayan orogen and found it to be good relative to other large-scale rainfall data sets available in the region. However, their analysis is potentially problematic because APHRODITE incorporates nearly all available station data, making it difficult to find independent station time series against which to test the accuracy of APHRODITE.

2.1.2. TMPA

Tropical Rainfall Measuring Mission (TRMM) Multisatellite Precipitation Analysis (TMPA)—3B42 V7 (TMPA) is a remotely sensed, gauge-adjusted, precipitation data set composed of measurements from several spaceborne instruments [*Huffman et al*., 2007] covering the globe from 50°N to 50°S and spanning from the beginning of 1998 to mid-2015 available at 3 h, daily, and monthly resolution. The data set integrates infrared and microwave observations from multiple satellites as well as ground-based gauge data [*Prakash et al*., 2015b]. We use the daily version of the product from 1998 to the end of 2013.

TMPA is known to have difficulties properly estimating the magnitude of rainfall in complex, steep terrain, though the new version V7 has improved in this regard [*Bharti et al*., 2016]. *Bharti et al*. [2016] also find that TMPA V7 does a good job estimating the frequency of large storms, but has difficulty accurately measuring their magnitude, commonly overestimating the storm magnitude below 3000 m and underestimating above 3000 m. In general it is also known to overestimate rainfall magnitudes in the Indian subcontinent [e.g., *Prakash et al*., 2015a]. Despite these shortcomings, TMPA outperforms all other available multisatellite products in the region [*Prakash et al*., 2014].

2.1.3. Quality of the Data Sets

While recognizing that both gridded data sets have potential issues, they are also the best currently available with a daily resolution [*Andermann et al*., 2011; *Prakash et al*., 2014]. In addition their respective weaknesses and strengths are complementary. APHRODITE is interpolated from accurate ground data, but suffers from a lack of stations. TMPA consists of measurements with a very high spatial resolution, but suffers from a lack of accuracy in the orogen. To mitigate the potential weaknesses of these data sets, we restrict our interpretations to features observed in both data sets and on a scale larger than the scale of the data set resolution.

2.2. Statistical Model

We define here the distribution of daily rainfall intensity to be the distribution of daily rainfall depths on days with rainfall exceeding 0.5 mm (wet days). The mean of this statistical distribution is referred to as the mean daily rainfall intensity (α). The mean rainfall rate including days with less than 0.5 mm of rainfall (wet days and dry days) is referred as the daily rainfall amount ($\mathbb{E}[P]$).The relationship between the two means is controlled by the ratio of wet days to the total number of days (λ) such that $\mathbb{E}[P]=\lambda\alpha$. We refer to λ as the mean wet day frequency. In order to describe the distribution of daily rainfall intensity (ignoring days with

less than 0.50 mm of rainfall), we use a PDF that can be fit to the empirical distribution. We searched for a model that is both simple (only a few, physically interpretable parameters) and flexible (it can fit well the empirical distribution over a wide range of climates). With only two parameters, the gamma distribution can fit the empirical distribution from markedly different climates. It also has a long history of application in modeling daily rainfall in general [e.g., *Eagleson*, 1978; *Srikanthan and McMahon*, 2001, and references therein], and in the Indian monsoon region specifically [e.g., *Mooley*, 1973; *Stephenson et al.*, 1999, and references therein; *May*, 2004a, and references therein; *May*, 2004b; *Mueller and Thompson*, 2013].

Due to the marked difference in daily rainfall intensity between the monsoon season and the dry season, we follow *Mueller and Thompson* [2013] and model the two seasons separately, so that the annual distribution is a mixture of distributions composed of one gamma distribution for the wet season and a second for the dry season, each weighted by the relative length of the associated season as shown in Figure 1. The resulting PDF, $f_P(p)$, has seven parameters—two daily rainfall intensity distributions with three parameters each and the length of the wet season.

$$f_P(p) = (1-\omega_w)\, f_d + \omega_w\, f_w, \tag{1}$$

where ω_w is the length of the wet season divided by 365, f_w is the daily rainfall intensity distribution for the wet season and f_d for the dry season. The distribution for the wet season is,

$$f_w(p) = (1-\lambda_w)\, \delta(p) + \lambda_w\, g(\beta_w, \gamma_w, p), \tag{2}$$

where $\delta(p)$ is the delta dirac function and $g(\beta_w, \gamma_w, p)$ is the gamma distribution,

$$g(\beta_w, \gamma_w, p) = \frac{\beta_w^{\gamma_w}}{\Gamma(\gamma_w)} p^{\gamma_w - 1} e^{-\beta_w p}, \tag{3}$$

where $\Gamma(\cdot)$ is the gamma function, β_w is the rate parameter, and γ_w is the shape parameter. The first term of equation (2) describes an atom of probability that the daily rainfall intensity is zero. The theoretical mean of the gamma distribution can be expressed as $\mathbb{E}[x] = \gamma_w/\beta_w$, which can be interpreted as the wet season mean rainfall intensity α_w.

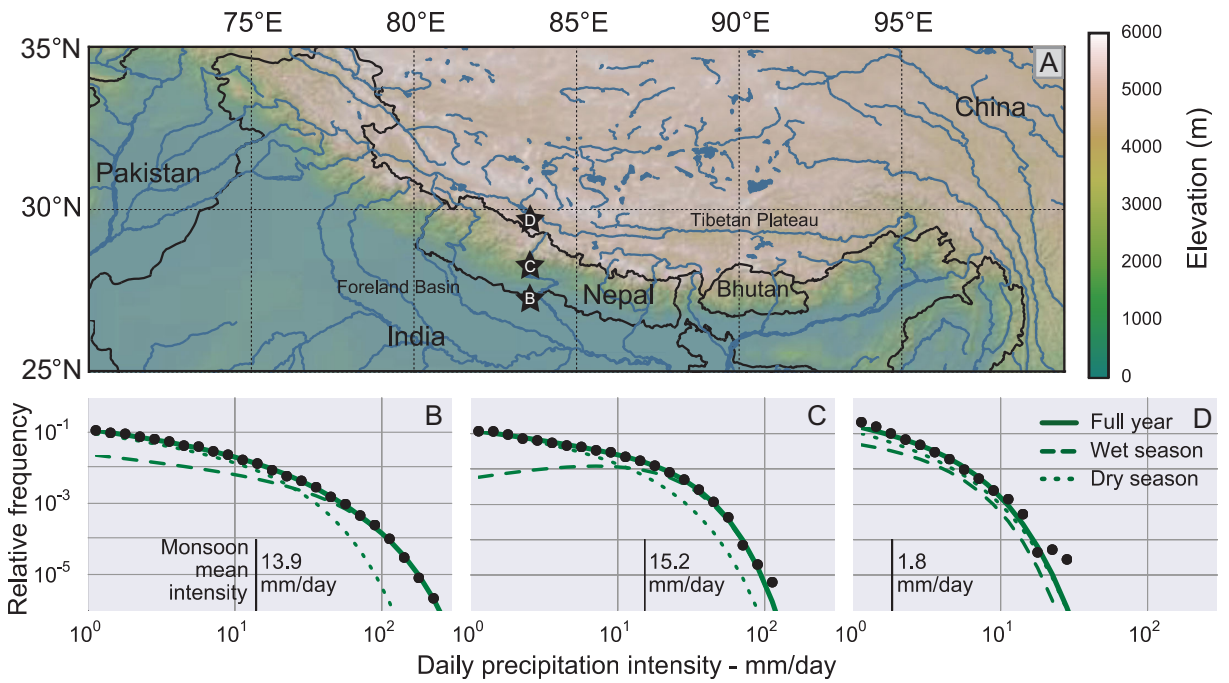

Figure 1. (a) Map of the region of interest. (b), (c), and (d) Examples of fitting the empirical distribution (black points). The plots correspond to the three black stars in Figure 1a. The full PDF is shown as a solid line, the monsoon season PDF as a dashed line, and the dry season as a dash-dotted line. Note the fundamental change in shape of the monsoon PDF from Figure 1b the southern band of high magnitude rainfall to Figure 1c the northern band, and Figure 1d the Tibetan plateau. The approximate location of the topographic divide is shown by the smoothed 3000, 4000, and 5000 m contour lines.

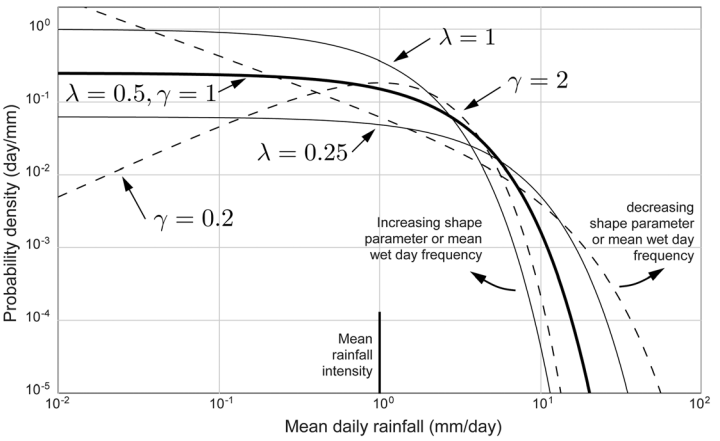

Figure 2. The effect of the gamma shape parameter and mean rainfall frequency on probability density functions (pdf) of daily rainfall intensity. The thick line shows a seasonal pdf with a shape parameter of 1 and a mean wet day frequency of 0.5. The thin solid lines show the effect of increasing or decreasing the mean wet day frequency λ to 1 and 0.25, respectively. The thin-dashed lines show the effect of increasing and decreasing the shape parameter γ across much of the observed range from 2 to 0.2. When either λ or γ are decreased, the magnitude of storms for low relative frequencies (e.g., $<10^{-2}$) increases though the total amount of rainfall does not.

The dry season daily rainfall intensity distribution has the identical form, where all parameters are subscripted with *d* instead of *w*. Because we are interested in the ability of the rainfall to drive erosion, we will focus exclusively on the wet season rainfall since it delivers a majority of the annual rainfall in much of the Himalayan orogen. All future references to the parameters of the gamma distribution refer to those from the wet season distribution.

In this model, the daily variability is described by two different parameters: the mean wet day frequency λ and the shape parameter γ. The first describes the likelihood of observing rainfall on a given day, with a lower likelihood of rain implying higher daily variability. This is very similar to how daily rainfall variability is quantified by *Tucker and Bras* [2000] or *Rossi et al.* [2016]. The second describes the variability of daily rainfall magnitude on days that have rainfall, with lower values implying higher variability in daily rainfall magnitude. Figure 2 shows how λ and γ separately affect the shape of the rainfall PDF. Knowing λ, γ, and α gives detailed information about the probability structure of daily rainfall for a given season. This allows for the computation of how often and by how much various geomorphic thresholds are expected to be exceeded in different climates. We can also use this model to estimate other statistics, such as the mean maximum annual storm magnitude (Appendix A).

There are several other distributions that are commonly used for wet day rainfall, such as the stretched exponential distributions [e.g., *Rossi et al.*, 2016], and we do not claim any strong theoretical reasons for using the gamma distribution over others. We make use of it because it fits the empirical distributions over the wide range of climates found in the Himalayan orogen, though it is probable that other distributions could do so as well.

2.3. Data Fitting Techniques

We estimate the model parameters described in section 2.2 for the distribution of daily rainfall at each node in both gridded data sets. To obtain estimates of the model parameters, we first created seasonal distributions by fitting a step function to the annual time series using the technique of *Mueller and Thompson* [2013]. The fitting of the step function is a simple method that provides an average start and end date for the wet season at each grid point. The results we obtain agree well with other assessments of the onset of the monsoon [*Wang*, 2002]. The seasonal mean wet day frequency was computed as the ratio of the number of days with more than 0.5 mm of rainfall to the total number of days in each season. We used maximum likelihood estimation to find the seasonal shape and rate parameters (Figure 3).

To assess the significance of our parameter estimation for the shape parameter and the rate parameter, we used the Fisher information to estimate the standard error (Figures 4a–4d). While useful, this only informs us about how probable the estimated parameters are under the assumption that the sample is gamma distributed. It does not inform us about how well the chosen gamma distribution fit the data; the best fitting gamma distribution may still fit poorly. To establish objectively the quality of the fit to observed daily rainfall distributions, we calculated the coefficient of determination, r^2, of a linear regression of the theoretical quantiles against the observed quantiles (Figures 4e and 4f) [*Müller et al.*, 2014].

$$r^2 = 1 - \frac{\sum_{i=1}^{N} (\hat{p}_i - p_i)^2}{\sum_{i=1}^{N} (p_i - \overline{p_i})^2}, \tag{4}$$

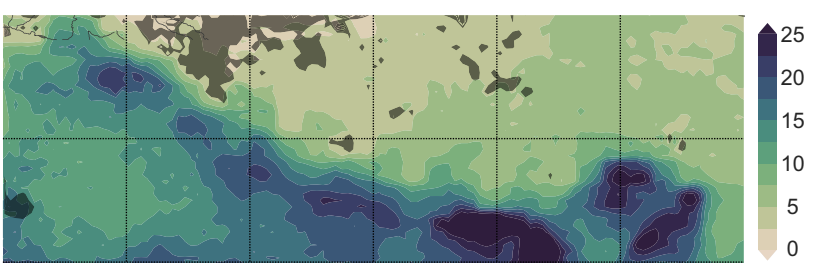
25
20
15
10
5
0

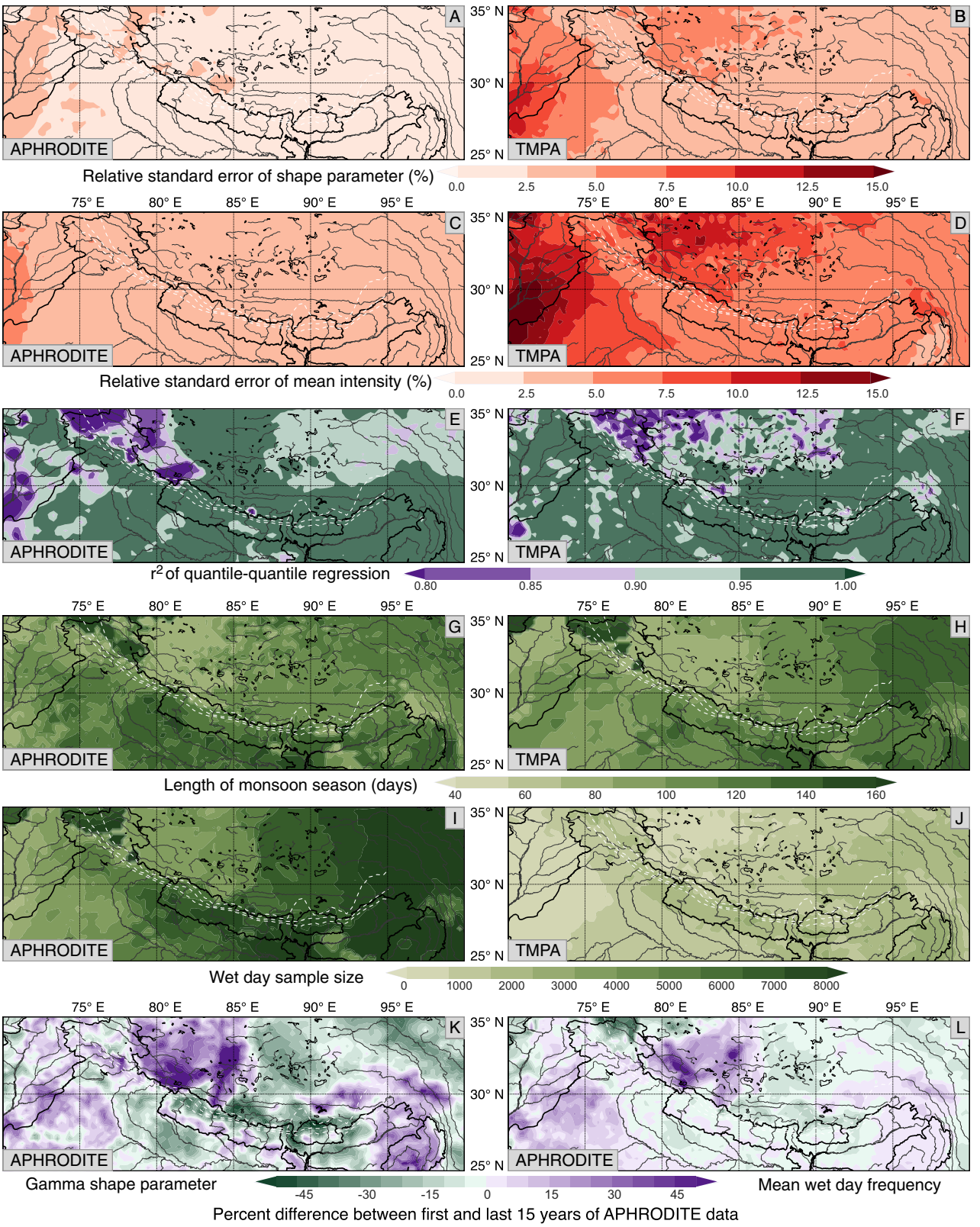

Figure 4. (a and b) Relative standard error for the shape parameter estimate, (c and d) relative standard error for mean daily intensity, (e and f) coefficient of determination, (g and h) estimate length of monsoon season, and (i and j) data set sample size for both APHRODITE and TMPA. (k and l) The percent difference between the first and last 15 years of the APHRODITE data set for the shape parameter and mean wet day frequency, respectively.

where N is the number of quantiles, p_i is the theoretical quantile, $\overline{p_i}$ is the observed quantile, and $\hat{p}_i$ is the mean of the theoretical quantiles. The closer r^2 is to one, the better the fit. We use all quantiles and, to be conservative, we reject all fits where $r^2 < 0.90$.

3. Results

The three estimated parameters, mean intensity, mean frequency, and wet day variability ($\hat{\alpha}_w$, $\hat{\lambda}_w$, and $\hat{\nu}_w$ respectively) are shown in Figure 3. Other aspects of the data analysis are shown in Figure 4. The standard error is low, with most estimates having less than 10% relative standard error (Figures 4a–4d). We note that the coefficient of determination (r^2) measuring the quality of the fit is for the most part above the 0.9 threshold we chose, though there are some poor fits on the Tibetan plateau, particularly in the west. Rejected fits are shown in Figure 3 as shaded regions. Also shown in Figure 4 is the length of the monsoon season as computed by fitting a step function to the annual rainfall time series, and the number of monsoon season wet day samples in each data set (Figures 4g–4l). The abrupt change in the length of the monsoon season in the western edge of the Himalayan orogen (34°N, 75°E) is associated with the breakdown of the dry season/monsoon season model due to the influence of significant winter rainfall. This results in a poor fit of the statistical model to empirical rainfall distributions and the low r^2 values in the region.

3.1. Spatial Distribution of the Gamma Shape Parameter

As discussed previously, the variability of daily rainfall is described by both the shape parameter and the mean wet day frequency. We find in this case that the range in the shape parameter is more significant than the range in the wet day frequency. Overall, the observed range of gamma shape parameter is between 0.1 and 4, with the majority of the values falling between 0.2 and 2. The range from 0.1 to 4 represents nearly an order of magnitude change in the size of the 99th percentile storm for a given mean rainfall amount, signalling a significant change in the variability of daily rainfall across the Himalayan orogen.

The spatial distribution of the gamma shape parameter, shown in Figures 3a and 3b, are qualitatively similar for both data sets across the Himalayan arc, though the range of values is smaller in the TMPA data set. The TMPA data set also exhibits higher wet day variability in western India, the southwestern edge of the Tibetan plateau and Pakistan. This may be due to the fact that the very low magnitude and frequency of rainfall in these areas allows them to be disproportionally affected by measurement errors.

Although the previous studies that measure the gamma shape parameter in a comparable manner do not focus on Himalayan rainfall and have a much coarser resolution, the general trends in shape parameters match well between all studies. *May* [2004a] and [2004b] shows large shape parameters along the Himalayan mountain front and *May* [2004b] and *Mooley* [1973] show small shape parameters in northwestern India and Pakistan, all observations which match our estimates well. More specifically, the magnitudes of the measured shape parameters from this study are very similar to *May* [2004a] and in particular, the reanalysis data set from *May* [2004b].

3.2. Spatial Distribution of Mean Wet Day Frequencies

The pattern of mean wet day frequencies, seen in Figures 3c and 3d, is broadly similar between the two data sets, though there are notable differences in the far western reaches of the range. The TMPA data set has in general higher wet day frequencies, though the frequencies are high overall in both data sets during the monsoon. The TMPA data set may exhibit higher frequencies because it is an areal measurement rather than a point measurement [*Del Jesus et al*., 2015]. In both data sets, frequencies are much higher closer to the bay of Bengal, the source of moisture for monsoonal rainfall, and fall off westward in the foreland basin. In contrast, wet day frequencies remain high for several thousand kilometers along the Himalayan mountain front where high relief has been shown to drive frequent rainfall [*Bookhagen and Burbank*, 2006]. Overall the estimated monsoon intensities and frequencies match well with previous analyses using large ground station data sets [*Stephenson et al*., 1999; *May*, 2004a, 2004b], and high spatial resolution remotely sensed data sets [*Bookhagen and Burbank*, 2006, 2010].

3.3. Spatial Distribution of Mean Storm Intensities

The mean rainfall intensities for the two data sets (Figures 3e and 3f) again have similar general trends, exhibiting high mean rainfall along the Himalayan mountain front. They also both measure low rainfall in

the Tibetan plateau and Pakistan. However, TMPA has higher magnitudes of daily rainfall intensity in general (note the different scale bars). The APHRODITE intensities are in agreement with estimates of intensity from three other studies, two using ground station data [*Stephenson et al*., 1999; *May*, 2004a] (4 and 89 years long, respectively), and a third using a reanalysis data set [*May*, 2004b]. The TMPA intensities agree well with intensities measured by GPCP, another satellite data set [*May*, 2004b].

3.4. Stationarity

Malik et al. [2016] demonstrate secular nonstationarity in daily rainfall in the Indian subcontinent. The main data set that they rely on for their analysis is derived from the same source as the APHRODITE data set we use here. Though their analysis of long-term trends is considerably more sophisticated, it is not surprising that we also find similar trends. Figures 4k and 4l show the difference in the shape parameter and the mean wet day frequency between the first 15 years (γ_F, λ_F) and the last 15 years (γ_L, λ_L) of the APHRODITE data set such that $\text{diff}(\gamma)=(\gamma_F-\gamma_L)/\gamma_L$ and $\text{diff}(\lambda)=(\lambda_F-\lambda_L)/\lambda_L$. There is a notable decrease in both the shape parameter and mean wet day frequency toward the present in the western Tibetan plateau (increase in variability), though this largely corresponds to regions where the statistical model we use does not work well, and therefore may be suspect. There is also a significant increase in the shape parameter in northern Nepal and Bhutan and moderate decrease in the shape parameter in southern Nepal. This implies that the pattern we observe in Nepal of a band of low variability in the north has increased in strength towards the present. The changes in variability implied by the observed shift in the mean wet day frequency and shape parameter match the changes in the distribution of rainfall across quantiles observed by *Malik et al*. [2016]. Though the number and distribution of stations from which the APHRODITE data are interpolated from has changed over the decades, and this may be partly responsible for the observed nonstationarity. Regardless, the main spatial trends in rainfall variability which we discuss in this study are observed in throughout the APHRODITE data set, even if their magnitudes shift, as well as in the TMPA data. One perspective is that the nonstationarity can be viewed as part of the variability, and we do not find it problematic that we implicitly include it in our measurement of daily variability. We are interested in the patterns of daily variability over periods of hundreds to thousands of years, which encompasses variation in measures of daily variability such as the shape parameter and mean wet day frequency which undoubtedly occur over decades and centuries.

3.5. Correlations Between Intensity, Frequency, and Shape Parameter

There is a strong negative correlation between the mean rainfall intensity and variability as measured by the frequency and the shape parameter. This is not surprising, because the shape parameter is related to the mean storm intensity via the scale parameter ($\alpha=\gamma_w/\beta_w$), and the mean wet day frequency is related to the mean rainfall intensity via the mean daily rainfall amount ($\mathbb{E}[P]=\alpha\lambda$). These negative correlations are shown in Figure 5. We have only shown the results from the TRMM data. The trends for the APHRODITE data are even stronger (steeper slopes and higher r^2 values) however, because the data are interpolated, there is the risk the observed correlations result in part from the interpolation.

We collapse the trends between mean rainfall intensity and mean wet day frequency at different elevations (Figure 5a) by normalizing both the intensity and the frequency for each elevation range by the mean value for that elevation range (Figure 5b). The result is a nondimensional relationship between the mean intensity and mean wet day frequency that is valid at all elevations in the Himalayan orogen ($1-\lambda \propto \alpha^b$). The positive correlation between the shape factor and mean intensity (Figure 5c) reflects a negative correlation between intensity and variability because increasing the shape parameter reduces the variability. We also collapse the trends at different elevations (Figure 5d), giving $\gamma \propto \alpha^b$. Notably, the slope b between all elevations is similar with the exception of elevations below 500 m, which includes much of the foreland basin and exhibits a weak relationship between mean intensity and variability. Given that both the shape parameter and the wet day frequency are strongly correlated with the mean intensity, it is not surprising that they are correlated with one another as well. Again we can collapse the trends at different elevation (Figure 5f), yielding a relationship of the form $\gamma \propto (1-\lambda)^b$.

These empirical relationships can potentially be used to relate the variability and intensity of rainfall to the mean annual rainfall amount at different elevations in a landscape evolution model of a monsoon dominated orogen. This is useful because it allows for the distribution of daily rainfall to be reconstructed with an estimate of the mean annual rainfall and estimates for the slopes (b) of the trends between intensity and variability.

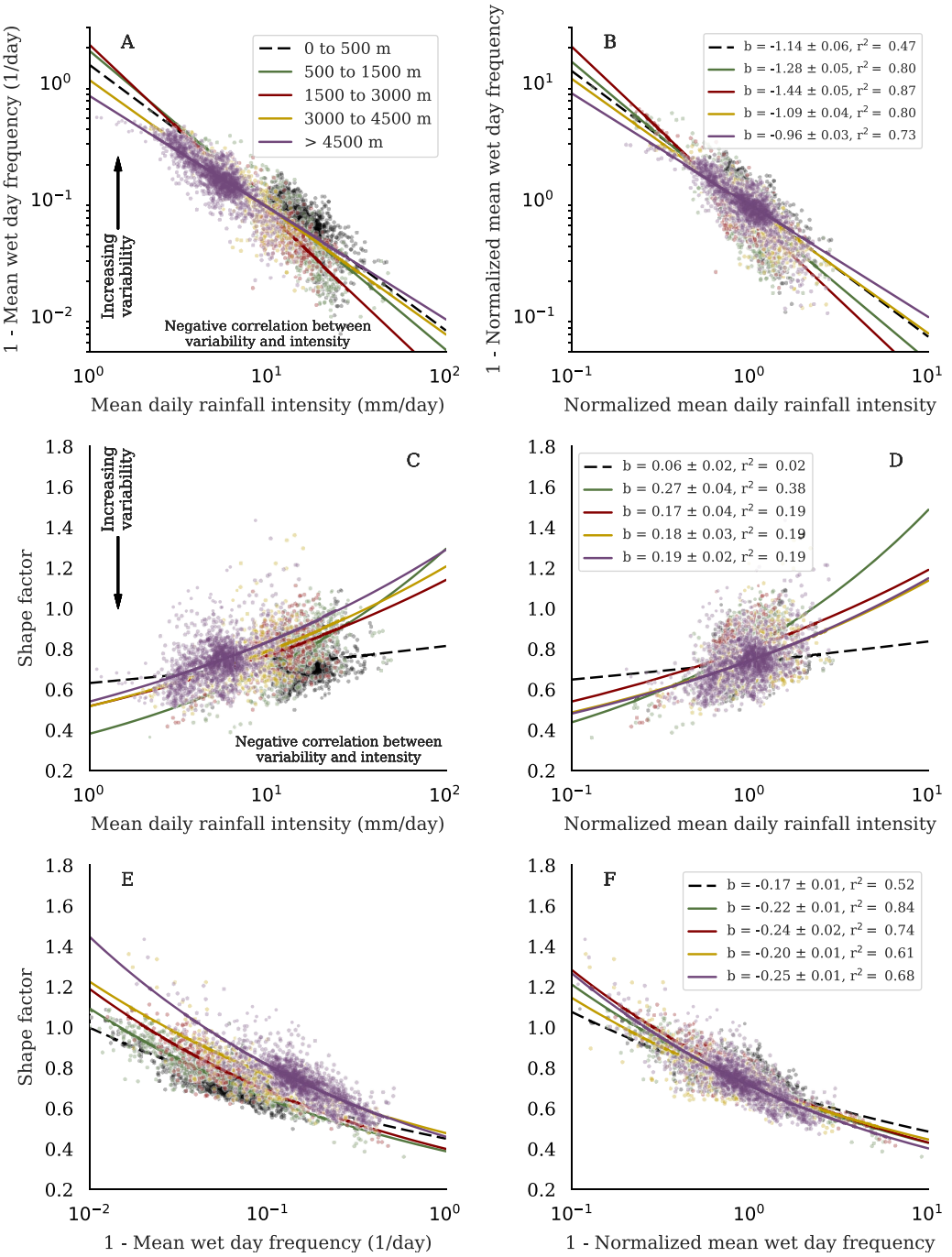

Figure 5. For the TMPA data set, (a) correlations between the mean wet day frequency and the mean rainfall intensity with trends fit to the data sorted by elevation. (b) The same, except the mean intensity and mean wet day frequency have been normalized by the mean value for each elevation range, collapsing the trends (normalized frequency – $(1-\lambda)/(1-\lambda_o)$ where λ_o is the mean value for each elevation range). (c) The correlation between the shape factor and the mean intensity, (b) which can be again collapsed by normalizing the mean intensity as in Figure 5b. (e and f) The same for the shape factor and the mean wet day frequency. In Figure 5f, the mean wet day frequency has been normalized as in Figure 5b.

3.6. General Along and Across Strike Trends in Variability

We observe large-scale trends in the shape parameter and mean wet day frequency both across and along the east-west strike of the orogen. These trends are shown in Figures 6a–6d, separated by elevation. We show only the TRMM data for the same reasons as before. The APHRODITE data show the same trends, with the difference that the variation in the shape parameter is much larger and the mean wet day frequencies

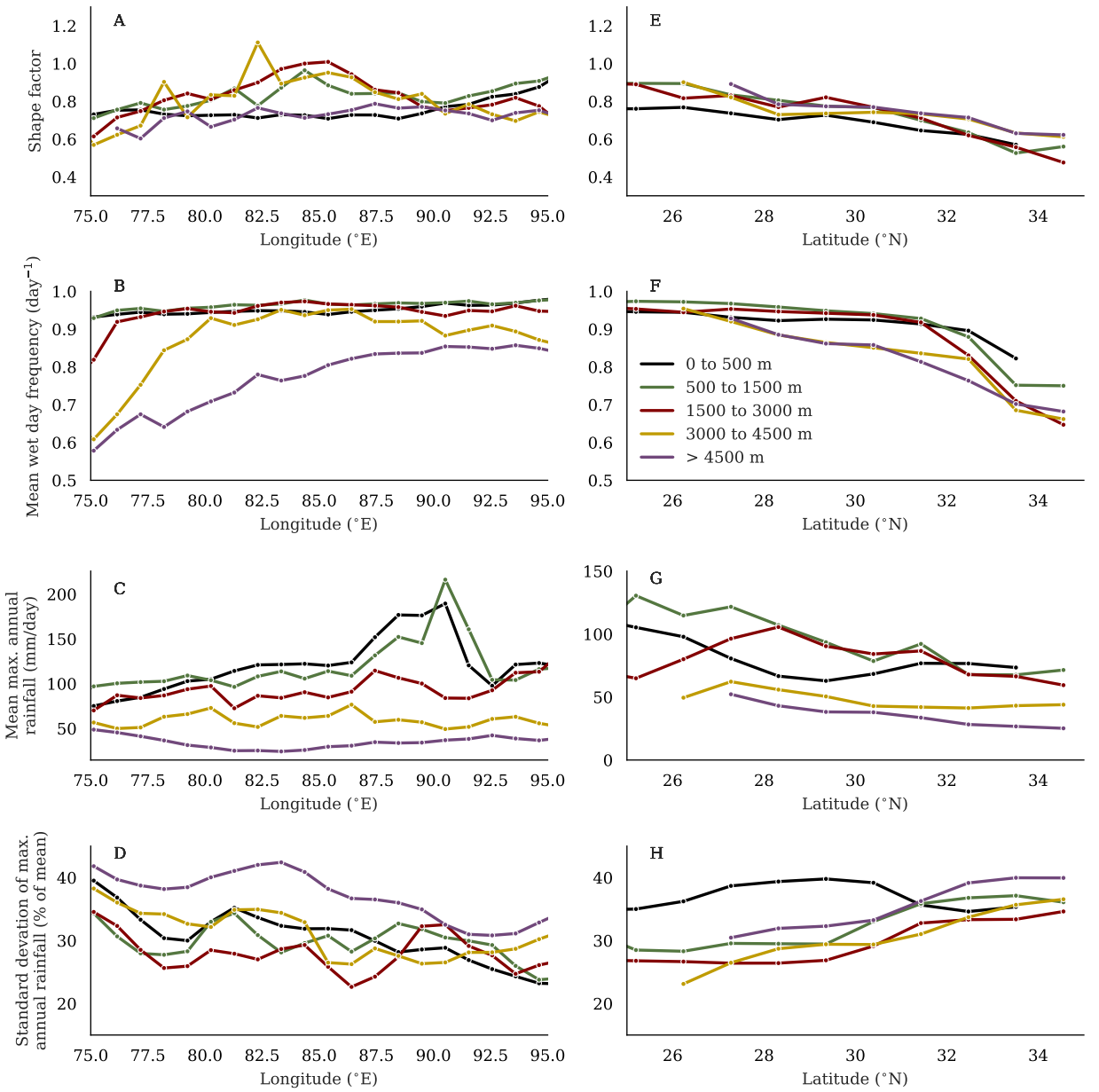

Figure 6. The average trends in the TMPA data along strike of the orogen from 75°E to 95°E of (a) the shape parameter, (b) the mean wet day frequency, (c) the mean maximum annual daily rainfall, and (d) the standard deviation of the max. annual daily rainfall. Shape parameters with $r^2 < 0.9$ has been left out of analysis. (e and f) The same respectively from 25°N to 35°N. In Figure 6d, the data has been smoothed by taking the running mean with a window size of 3.

somewhat lower. Along strike from east to west, both the shape parameters (Figure 6a) and the mean wet day frequencies (Figure 6c) increase at all elevations above 500 m. Below 500 m, both the shape parameter and the mean wet day frequency are relatively constant. At moderate and high elevations (500–4500 m), the shape parameter reaches peak values at around 85°E, after which it decreases again, but even at these elevations, the shape parameters in the east are still larger than in the west. Because increases in either the mean wet day frequency or the shape parameter imply a decrease in rainfall variability, it can be seen that the variability is highest in the west and decreases to the east with a low in variability at around 85°E at some elevations. Similar trends exist across strike. At all elevations both shape parameter and mean wet day frequency decrease to the north (Figures 6b and 6d, respectively). Therefore, in general the variability of daily rainfall during the monsoon is lowest in the east and the south of the orogen, and increases both northward and westward. This is opposite to the pattern of rainfall mean and intensity, which is

unsurprising, given the strong negative correlation between daily intensity and both the shape parameter and mean wet day frequency.

The mean rainfall amount and intensity decrease toward the west from the source of moisture, the bay of Bengal, in the east. However, because of the increasing rainfall variability at elevations above 500 m (as shown by both the frequency and shape parameter), the magnitude of the average maximum annual daily rainfall is nearly constant at those elevations (Figure 6e). At elevations above 4500 m, the magnitude of the average maximum annual daily rainfall increases toward the west from a minimum at around 83°E. *Wulf et al*. [2016] found a bias in the TMPA data that causes rainfall to be overestimated in the dry, high relief regions in the west of the orogen. This bias could potentially cause the trend seen here. However, the APHRODITE data, which will not be influenced by this bias, exhibits the same trend. In fact, in the APHRODITE data, the average maximum annual daily rainfall magnitude increases slightly for all elevations above 500 m rather than remaining constant.

Figures 6g and 6h show the standard deviation of the maximum annual daily rainfall as a percent of the maximum annual daily rainfall. It is relatively constant from east to west, perhaps increasing slightly in the west, however from south to north it can be seen to increase modestly. This means that in the orogen interior, storms with return times longer than a year can be larger with respect to the mean rainfall intensity than in the south, reflecting the higher variability in the north and highlighting that big storms are likely to be very significant in the relatively dry orogen interior.

4. Discussion

4.1. Rainfall Variability and Erosion Rates

The relative importance and impact of the intensity and variability of daily rainfall will depend on the details of the erosion regime in question, with emphasis on the kind and magnitude of erosion threshold or nonlinearity considered. For an erosion threshold associated with a minimum storm size or a nonlinearity which disproportionally weights larger storms, higher variability rainfall will lead to higher erosion rates. This is thought to be the case for erosion occurring in mountainous bedrock rivers [*Tucker and Bras*, 2000; *Tucker*, 2004; *Snyder et al*., 2003; *Lague*, 2005; *DiBiase and Whipple*, 2011]. River erosion is far from the only erosion process occurring in the Himalayan orogen, but it is generally considered to be one of the most significant in active orogens [e.g., *Whipple*, 2004; *Molnar*, 2001], especially considering the minor influence of glaciers and glacial erosion in central Nepal. Due to the complexity of hydrological processes, it is challenging to link daily rainfall distributions to daily streamflow distributions. Empirical work investigating the drivers of daily streamflow find a number environmental controls, including the evapotranspiration rate and aridity index [*Rossi et al*., 2016]. Importantly, they find a positive correlation between the wet day frequency and streamflow variability, and to a lesser extent between rainfall variability (i.e., the shape parameter) and streamflow variability. Using numerical simulations, another study found that the shape parameter of daily rainfall could have a significant impact on streamflow variability when the shape parameter is less than 0.5 [*Müller et al*., 2014].

4.2. Relevance to the Himalayan Orogen

One of the more striking features of the spatial distribution of the shape parameter and the wet day frequency in Figure 3 is the 1000 km long arc along the crest of the Himalayan orogen, particularly strong in Nepal. This band appears in both data sets, and corresponds with the northern most of the two bands of high magnitude rainfall described by *Anders et al*. [2006] and *Bookhagen and Burbank* [2006]. The large shape parameter and high wet day frequency imply that the northern band of high magnitude rainfall is characterized by low variability rainfall. In contrast, the southern band possesses moderate to high variability along its length. Therefore the two bands of rainfall, while similar in mean intensity of daily rainfall, overall rainfall amount, and topographic setting, differ greatly in the frequency and magnitude of rainfall during the monsoon. This is supported by *Bookhagen and Burbank* [2010] who use both the frequency of lightning strikes (a feature of extreme rainfall events) and the intensity of rainfall during extreme events to characterize the magnitude of extreme events and find a maximum of extreme events along the front of the Himalayan arc, over the southern rainfall band.

4.2.1. Patterns of Variability and Long-Term Erosion Rates

The band of low rainfall variability may help to explain the inconsistency between measured long-term erosion rates and rainfall rates in the region. *Burbank et al*. [2003] and *Thiede and Ehlers* [2013] showed that in

central Nepal, erosion rates increase north of the band of high magnitude rainfall. It can be seen that mean erosion rate increases even as the mean rainfall rate decreases. Erosion rates inferred from cooling ages peak close to the topographic divide, well north of the highest mean rainfall rates. If the region is in dynamic equilibrium, we expect the erosion rate to be set by the uplift rate rather than climate. However, the specific stream power should still reflect the erosion rate. In this region the specific stream power still decreases northward (albeit more slowly that rainfall) [*Burbank et al.*, 2003]. This implies that steeper slopes and narrower channels can make up only partially for the decreasing rainfall. Increasing rainfall variability could explain some of the discrepancy between erosion rates and rainfall rates. Figure 7a shows a representative cross section over the topographic divide in this region. The rainfall variability increases rapidly as the

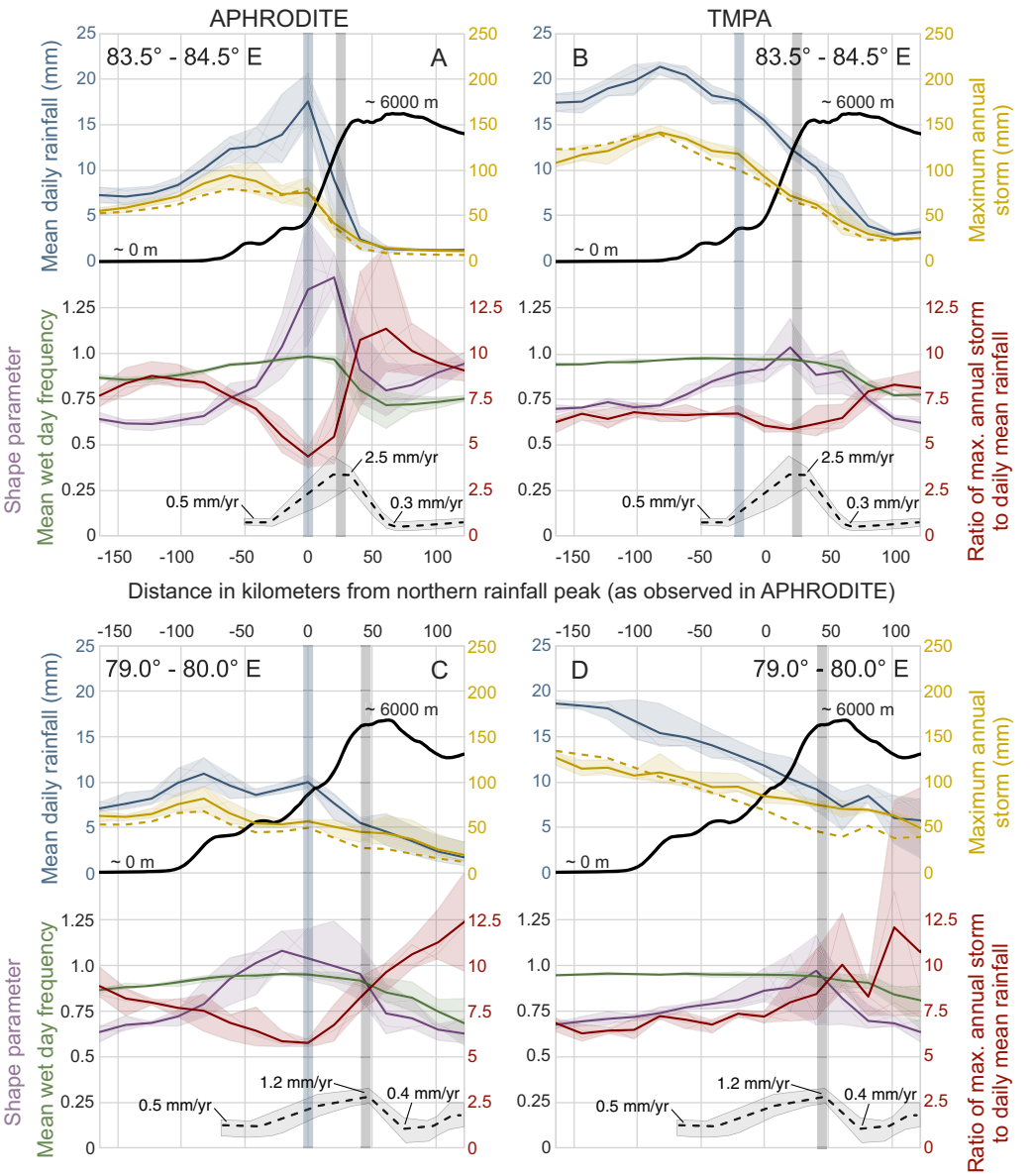

Figure 7. Representative cross sections orthogonal to the strike of the orogen showing the patterns of daily rainfall mean and variability across the topographic divide. Cross sections are aligned relative to the location of the northern rainfall peak. The lines show the average value across the section, and the shaded regions show the range. The mean daily rainfall rate is shown in blue, the mean maximum annual storm is shown in solid yellow, the estimated maximum annual storm is shown in dashed yellow, the ratio of the daily mean to the annual max. Storm is shown in red, the gamma shape parameter is shown in purple and the mean wet day frequency is shown in green. Vertical bars show peak of erosion rate (as inferred from cooling ages) and mean rainfall rate (gray and blue resp.). Estimated erosion rates over the last 2 million years obtained from a 1-D inversion of thermochronological data taken from *Thiede and Ehlers* [2013] are shown with the dashed black line. Average maximum topography shown as solid black line.

mean rainfall rate decreases across the topographic divide, as demonstrated by the observed decrease in the shape parameter and mean wet day frequency. The observed increase in rainfall variability, in conjunction with narrowing channels and steepening slopes, is consistent with a peak erosion rate on the topographic divide despite significantly decreasing mean rainfall rate. As further support for this, both steeper slopes and higher rainfall variability are expected to enhance other important erosion processes, such as landsliding [*Gabet et al*., 2004].

Increasing rainfall variability means that while the total amount of rainfall decreases sharply across the topographic divide, the size of large storms will decreases more slowly. The solid yellow line in Figures 7a and 7b show the average maximum annual storm size, and it can be seen that it does not track with the mean daily rainfall rate, and does decrease more slowly across the divide. More than that, the east-west striking band of very low variability associated with the northern band of high rainfall results in the large storms in this region being exceptionally small given the high rainfall rate. The ratio of the mean maximum annual storm to the mean daily rainfall rate can be used as another measure of rainfall variability. Shown as the solid red line in Figure 7, we see that it is consistent with the measured changes in the shape parameter and mean wet day frequency. It is very low over the northern band of high magnitude rainfall, and highest over the Tibetan plateau. Figures 7c and 7d show another representative cross section further to the west near the end of the arc of low variability. The same pattern holds for this cross section as well, with increasing variability across the topographic divide, reflected both in the ratio of the maximum annual storm to the daily mean rainfall as well as the shape parameter and wet day frequency. In this cross section, the rise in topography from south to north is gentler, as are the gradients in the erosion rate, mean daily rainfall, mean wet day frequency, and the shape parameter.

We put forth the idea of rainfall variability resolving the inconsistency between long-term erosion rate and rainfall rate only as a possibility. The theoretical arguments provide a basis for this theory, and the APHRODITE data support it. However, it is not possible to rule out that the modern climate is a poor representation of past climate. However, the current climatic regime results from moisture laden air brought by the Indian monsoon colliding with high relief topography (the southern edge of the Tibetan plateau) [*Bookhagen and Burbank*, 2006]. Both the plateau and the Indian monsoon are estimated to have existed in their current form for the last 8 million years [*Zhisheng et al*., 2001]. Though the strength of the monsoon has changed through time, this implies that the current climate should be roughly representative of climatic forcing in the region over the last few million years, and lends credence to the idea that the Himalayan orogen is in dynamic equilibrium.

A further concern is that the way that rainfall drives erosion rates across the landscape is not perfectly understood. So we must restrict ourselves to a qualitative assessment of the patterns of rainfall variability and mean. It is not clear how to assess whether the magnitude of increase in variability is sufficient to offset the magnitude of decrease in mean rainfall. Additionally, the TMPA data (Figures 7b and 7d) only broadly match the pattern observed in the APHRODITE data set (Figures 7a and 7c). The rise in variability observed in the TMPA data occurs further north than in the APHRODITE data, and is not coincident with the peak in the erosion rate. Further, the TMPA data do not resolve the northern rainfall maximum, making it more difficult to compare the peak in erosion to rainfall. Due to this, in the Nepal swath (Figure 7b) the TMPA data do not support the theory that increasing rainfall variability offsets decreasing rainfall mean (though they do in swath Figure 7d). Additionally the elevation is an important parameter in the interpolation scheme of the APHRODITE data, making swath profiles with the APHRODITE data suspect.

One point in support of the theory comes from a data set derived from the TMPA 2B31 data that has much higher spatial resolution that the ones we used here *Bookhagen and Burbank* [2006, 2010]; *Bookhagen* [2010]; and *Olen et al*. [2016]. The TMPA-derived data resolve the northern peak in rainfall magnitude and low in variability in a very similar location to the APHRODITE data (B. Bookhagen, personal communication). This lends support to the APHRODITE data. So, while we find the data presented here is suggestive that rainfall variability may be a key parameter influencing the erosion efficiency of rainfall in the Himalayan orogen, we conclude that better data, which may become available in the future, are necessary to confirm or refute this hypothesis.

4.2.2. Patterns of Variability and Short-Term Erosion Rates

Olen et al. [2016] conducted an analysis of the empirical relationships between vegetation density, precipitation rates, and short-term denudation rates in the Himalayan orogen. They find a strikingly clear negative

correlation between vegetation density and the variability of measured denudation rates within a single basin. The lower the vegetation density, the higher the variation in measured denudation rates. They point out the logic in this; vegetation tends to stabilize soils, increasing the resistance to erosion. Basins with low vegetation density should be more vulnerable to substantial surface erosion during large rainstorms than those with high vegetation density. The erosion caused by large rainstorms will likely not be evenly distributed across the basin for a variety of reasons including localized high intensity rainfall, nonuniformly distributed vegetation, and different antecedent conditions on different hillslopes. This will lead to more episodic, localized erosion events, and consequently, more variation in denudation rates measured within a single basin or region.

It is also logical that rainfall variability would influence this trend by increasing the size and frequency of large storms in regions with high rainfall variability relative to those with low variability. *Olen et al*. [2016] therefore also compare rainfall variability to denudation variability and vegetation density. However, while they observe vegetation density to increase and denudation variability to decrease from west to east along the strike of the orogen, they find rainfall variability trends in the opposite sense, increasing from west to east. *Olen et al*. [2016] use the number of times per year that extreme events occur as a measure of variability, where extreme events are defined by them as events above the 90th percentile. This does not match the decrease in denudation variability from west to east, and they conclude that the influence of increasingly dense vegetation toward the east is so strong as to erase any effects of increasing rainfall variability on denudation variability. While we agree completely with their explanation of how vegetation density and rainfall variability are likely to influence the variation in measured denudation rates, we offer different perspective on the trend of variability. This is based on the observation that the shape parameter and mean wet day frequency decrease from east to west, implying an increase variability from east to west rather than west to east.

The potential problem with using the number of events above the 90th percentile as a measure of daily rainfall variability is that there is not a standard relationship between the magnitude of the 90th percentile event and the mean rainfall intensity. This is determined by the shape parameter of the distribution and varies from region to region. Figure 8 shows the mean magnitude of events above the 90th percentile as a function of the shape parameter. As the shape parameter falls below one, the average magnitude of extreme events approaches 10 times the mean rainfall intensity, but above one, it is only about 2–3 times the mean. Therefore, right where there are the most frequent extreme events, in central Nepal, is where those extreme events will be the least intense. This is an important point, because from geomorphological perspective, it is not just the frequency of large storms that is important, but also their magnitude. The shape parameter and mean wet day frequency can be used to measure the magnitude of these storms relative to the mean rainfall intensity in an unbiased way that allows for comparison between regions with significantly different mean rainfall intensities (such as central Nepal and the Tibetan plateau).

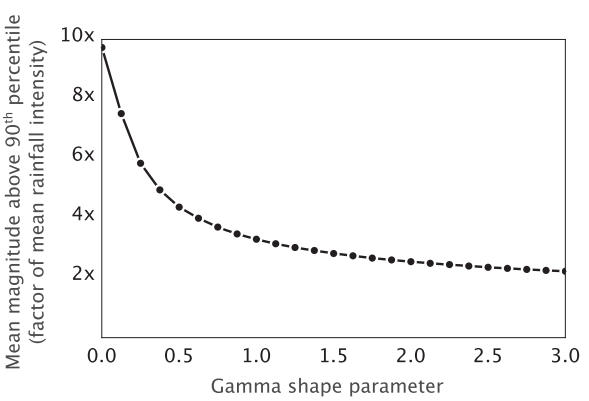

Figure 8. The change in the mean magnitude of daily rainfall above the 90th percentile as a function of the shape parameter. When the shape parameter is less than 0.5, the average intensity of storms above the 90th percentile is 5 to 10 times the mean rainfall intensity. For shape parameters above one, the average intensity of storms above the 90th percentile is only about 2–3 times the mean rainfall intensity.

As Figure 6 shows, these measures of variability point to an increase in variability from the east to the west and from the south to the north of the orogen. This is more consistent with the patterns of denudation variability and vegetation density observed by *Olen et al*. [2016]. Moving along the orogen from east to west, the mean annual rainfall drops, as does the mean rainfall intensity and the vegetation density. At the same time the variability of rainfall and the variability in denudation increase. As Figure 6c shows, the maximum annual storm magnitude does not change along strike for most elevations, because of increasing rainfall variability. As a result, large storms become more extreme relative the mean rainfall intensity. It is unsurprising that the most episodic erosion

is observed in the west. However, whether the denudation variability increases to the west because of increasingly significant large storms, or because of decreasing vegetation density or both is less clear.

We point out however, that our conclusions are based on monsoon rainfall only, while they analyze annual precipitation. Winter precipitation increases to the east along strike. As a result, monsoon rainfall is less representative of the annual precipitation patterns in the east as compared to the west. Further, the existence of winter precipitation and spring snowmelt could decrease the variability of delivery water to the ecosystem.

5. Conclusions

In this study, we have made a careful characterization of the distribution of rainfall in the Himalayan orogen. We find a consistent pattern appearing with the gamma shape parameter, mean wet day frequency, and mean rainfall intensity in many places along the Himalayan arc, particularly in Nepal. We observe moderate rainfall variability in the foreland basin up to and including the southern band of high magnitude rainfall. This is where the biggest storms are taking place during the monsoon as the moist air coming from the bay of Bengal collides with the first rapid rise in topography and relief [*Bookhagen and Burbank*, 2006]. Although a significant amount of moisture makes it past the initial mountain front to collide with the second steep rise in topography and relief near the topographic divide and form the northern band of high magnitude rainfall, the storms there are not as intense. Instead a more frequent, more moderate rainfall regime is observed. This is reflected in the rainfall variability which begins to drop rapidly starting at the southern band moving north, and reaches a low right at or directly north of the northern band. Further into the orogen from the northern band, mean rainfall amount decreases rapidly while variability increases due to both the mean wet day frequency and the shape parameter. In general the plateau directly behind the mountains possesses moderate to high rainfall variability. Similarly, while the mean monsoonal rainfall amount and intensity decrease along strike from east to west, the rainfall variability increases. As a result, the magnitude of moderate to large storms remains constant along the strike of the orogen above 500 m elevation. These two trends point to monsoonal rainfall having a larger geomorphic impact in the north and the west of the orogen than the mean rainfall intensity and amount suggest. This demonstrates the potential importance of rainfall variability in understanding the relationship between erosion and climate.

Appendix A: Mean Maximum Annual Storm

We can use the statistical model to predict the average maximum annual storm. We obtain this from the mean of the probability distribution of the maximum annual storm magnitude. This is equivalent to the probability of exceeding a given storm size p over the course of a year, which is the joint probability of exceeding p on each day of the year. Rainfall is assumed to be independent from day to day, so $F_{\max}(p)$ is the probability to exceed a storm size of p on a given day raised to the power n, where n is the number of rainy days per year. Therefore, $F_{\max}(p)=\Pr[x \geq p]^n=F(p)^n$, where $F(p)=\Gamma(\gamma, \beta p)$ is the cumulative distribution function of the gamma distribution and $\Gamma(\cdot,\cdot)$ is the regularized upper incomplete gamma function. We assume that the monsoon season will always contribute the largest storm of the year, so the average maximum annual storm is $P_{\max}=\mathbb{E}[\Gamma(\gamma_w, \beta_w p)^{n_w}]$, where $n_w=\lambda_w \omega_w \cdot 365$ is the mean number of rainy days in the monsoon season.

Acknowledgments
This work was supported by an inter-European research group. The APHRODITE data set used in this study is freely available at http://www.chikyu.ac.jp/precip/index.html. The TMPA data set used in this study is freely available at http://TMPA.gsfc.nasa.gov/data_dir/data.html.

References

Adlakha, V., K. A. Lang, R. C. Patel, N. Lal, and K. W. Huntington (2013), Rapid long-term erosion in the rain shadow of the Shillong Plateau, Eastern Himalaya, *Tectonophysics*, *582*, 76–83.

Andermann, C., S. Bonnet, and R. Gloaguen (2011), Evaluation of precipitation data sets along the Himalayan front, *Geochem. Geophys. Geosyst.*, *12*, Q07023, doi:10.1029/2011GC003513.

Andermann, C., A. Crave, R. Gloaguen, P. Davy, and S. Bonnet (2012), Connecting source and transport: Suspended sediments in the Nepal Himalayas, *Earth Planet. Sci. Lett.*, *351–352*, 158–170.

Anders, A. M., G. H. Roe, B. Hallet, D. R. Montgomery, N. J. Finnegan, and J. Putkonen (2006), Spatial patterns of precipitation and topography in the Himalaya, *Geol. Soc. Am. Spec. Pap.*, *398*, 39–53.

Beer, A. R., and J. M. Turowski (2015), Bedload transport controls bedrock erosion under sediment-starved conditions, *Earth Surf. Dyn.*, *3*, 291–309.

Bharti, V., C. Singh, J. Ettema, and T. Turkington (2016), Spatiotemporal characteristics of extreme rainfall events over the northwest Himalaya using satellite data, *Int. J. Climatol.*, *36*, 3949–3962.

Bookhagen, B. (2010), Appearance of extreme monsoonal rainfall events and their impact on erosion in the Himalaya, *Geomat. Nat. Hazards Risk*, *1*, 37–50.
Bookhagen, B., and D. Burbank (2006), Topography, relief, and TRMM-derived rainfall variations along the Himalaya, *Geophys. Res. Lett.*, *33*, L08405, doi:10.1029/2006GL026037.
Bookhagen, B., and D. Burbank (2010), Toward a complete Himalayan hydrological budget: Spatiotemporal distribution of snowmelt and rainfall and their impact on river discharge, *J. Geophys. Res.*, *115*, F03019, doi:10.1029/2009JF001426.
Burbank, D. W., A. E. Blythe, J. Putkonen, B. Pratt-Sitaula, E. Gabet, M. Oskin, A. Barros, and T. P. Ojha (2003), Decoupling of erosion and precipitation in the Himalayas, *Nature*, *426*, 652–655.
Burbank, D. W., B. Bookhagen, E. J. Gabet, and J. Putkonen (2012), Modern climate and erosion in the Himalaya, *C. R. Geosci.*, *344*, 610–626.
Burgueño, A., M. D. Martinez, C. Serra, and X. Lana (2010), Statistical distributions of daily rainfall regime in Europe for the period 1951–2000, *Theor. Appl. Climatol.*, *102*, 213–226.
Caloiero, T. (2014), Analysis of daily rainfall concentration in New Zealand, *Nat. Hazards*, *72*, 389–404.
Craddock, W. H., D. W. Burbank, B. Bookhagen, and E. J. Gabet (2007), Bedrock channel geometry along an orographic rainfall gradient in the upper Marsyandi River valley in central Nepal, *J. Geophys. Res.*, *112*, F03007, doi:10.1029/2006JF000589.
Dadson, S. J., et al. (2003), Links between erosion, runoff variability and seismicity in the Taiwan orogen, *Nature*, *426*, 648–651.
Del Jesus, M., A. Rinaldo, and I. Rodríguez-Iturbe (2015), Point rainfall statistics for ecohydrological analyses derived from satellite integrated rainfall measurements, *Water Resour. Res.*, *51*, 2974–2985, doi:10.1002/2015WR016935.
DiBiase, R. A., and K. X. Whipple (2011), The influence of erosion thresholds and runoff variability on the relationships among topography, climate, and erosion rate, *J. Geophys. Res.*, *116*, F04036, doi:10.1029/2011JF002095.
DiBiase, R. A., K. X. Whipple, A. M. Heimsath, and W. B. Ouimet (2010), Landscape form and millennial erosion rates in the San Gabriel Mountains, CA, *Earth Planet. Sci. Lett.*, *289*, 134–144.
Dietrich, W. E., C. J. Wilson, D. R. Montgomery, and J. McKean (1993), Analysis of erosion thresholds, channel networks, and landscape morphology using a digital terrain model, *J. Geol.*, *101*, 259–278.
Eagleson, P. S. (1978), Climate, soil, and vegetation: 2. The distribution of annual precipitation derived from observed storm sequences, *Water Resour. Res.*, *14*, 713–721.
Gabet, E. J., D. W. Burbank, J. K. Putkonen, B. A. Pratt-Sitaula, and T. Ojha (2004), Rainfall thresholds for landsliding in the Himalayas of Nepal, *Geomorphology*, *63*, 131–143.
Godard, V., D. L. Bourlès, F. Spinabella, D. W. Burbank, B. Bookhagen, G. B. Fisher, A. Moulin, and L. Léanni (2014), Dominance of tectonics over climate in Himalayan denudation, *Geology*, *42*, 243–246.
Hirschmiller, J., D. Grujic, B. Bookhagen, I. Coutand, P. Huyghe, J. L. Mugnier, and T. Ojha (2014), What controls the growth of the Himalayan foreland fold-and-thrust belt?, *Geology.*, *42*, 247–250.
Horton, R. (1945), Erosional development of streams and their drainage basins; hydrophysical approach to quantitative morphology, *Geol. Soc. Am. Bull.*, *56*, 275–370.
Huffman, G., D. Bolvin, E. Nelkin, D. Wolff, R. Adler, G. Gu, Y. Hong, K. Bowman, and E. Stocker (2007), The TRMM Multisatellite Precipitation Analysis (TMPA): Quasi-global, multiyear, combined-sensor precipitation estimates at fine scales, *J. Hydrometeorol.*, *8*, 38–55.
Jiang, P., D. Wang, and Y. Cao (2016), Spatiotemporal characteristics of precipitation concentration and their possible links to urban extent in china, *Theor. Appl. Climatol.*, *123*, 757–768.
Joshi, S., K. Kumar, V. Joshi, and B. Pande (2014), Rainfall variability and indices of extreme rainfall-analysis and perception study for two stations over central Himalaya, India, *Nat. Hazards*, *72*, 361–374.
Lague, D. (2005), Discharge, discharge variability, and the bedrock channel profile, *J. Geophys. Res.*, *110*, F04006, doi:10.1029/2004JF000259.
Lague, D. (2014), The stream power river incision model: Evidence, theory and beyond, *Earth Surf. Processes Landforms*, *39*, 38–61.
Malik, N., B. Bookhagen, and P. J. Mucha (2016), Spatiotemporal patterns and trends of Indian monsoonal rainfall extremes, *Geophys. Res. Lett.*, *43*, 1710–1717, doi:10.1002/2016GL067841.
Martin-Vide, J. (2004), Spatial distribution of a daily precipitation concentration index in peninsular Spain, *Int. J. Climatol.*, *24*, 959–971.
May, W. (2004a), Variability and extremes of daily rainfall during the Indian summer monsoon in the period 1901-1989, *Global Planet. Change*, *44*, 83–105.
May, W. (2004b), Simulation of the variability and extremes of daily rainfall during the Indian summer monsoon for present and future times in a global time-slice experiment, *Clim. Dyn.*, *22*, 183–204.
Molnar, P. (2001), Climate change, flooding in arid environments, and erosion rates, *Geology*, *29*, 1071–1074.
Mooley, D. A. (1973), Gamma distribution probability model for Asian summer monsoon monthly rainfall, *Mon. Weather Rev.*, *101*, 160–176.
Mueller, M. F., and S. E. Thompson (2013), Bias adjustment of satellite rainfall data through stochastic modeling: Methods development and application to Nepal, *Adv. Water Resour.*, *60*, 121–134.
Müller, M. F., D. N. Dralle, and S. E. Thompson (2014), Analytical model for flow duration curves in seasonally dry climates, *Water Resources Research*, *50*, 5510–5531, doi:10.1002/2014WR015301.
Olen, S. M., B. Bookhagen, and M. R. Strecker (2016), Role of climate and vegetation density in modulating denudation rates in the Himalaya, *Earth Planet. Sci. Lett.*, *445*, 57–67.
Prakash, S., V. Sathiyamoorthy, C. Mahesh, and R. Gairola (2014), An evaluation of high-resolution multisatellite rainfall products over the Indian monsoon region, *Int. J. Remote Sens.*, *35*, 3018–3035.
Prakash, S., A. K. Mitra, A. AghaKouchak, and D. Pai (2015a), Error characterization of TRMM Multisatellite Precipitation Analysis (TMPA-3B42) products over India for different seasons, *J. Hydrol.*, *529*, 1302–1312.
Prakash, S., A. K. Mitra, and D. Pai (2015b), Comparing two high-resolution gauge-adjusted multisatellite rainfall products over India for the southwest monsoon period, *Meteorol. Appl.*, *22*, 679–688.
Prosser, I. P., and W. E. Dietrich (1995), Field experiments on erosion by overland flow and their implication for a digital terrain model of channel initiation, *Water Resour. Res.*, *31*, 2867–2876.
Rossi, M. W., K. X. Whipple, and E. R. Vivoni (2016), Precipitation and evapotranspiration controls on daily runoff variability in the contiguous United States and Puerto Rico, *J. Geophys. Res. Earth Surface*, *121*, 128–145, doi:10.1002/2015JF003446.
Scherler, D., B. Bookhagen, and M. R. Strecker (2014), Tectonic control on 10Be-derived erosion rates in the Garhwal Himalaya, India, *J. Geophys. Res. Earth Surface*, *119*, 83–105, doi:10.1002/2013JF002955.
Snyder, N. P., K. X. Whipple, G. E. Tucker, and D. J. Merritts (2003), Importance of a stochastic distribution of floods and erosion thresholds in the bedrock river incision problem, *J. Geophys. Res.*, *108*(B2), 2117, doi:10.1029/2001JB001655.
Srikanthan, R., and T. A. McMahon (2001), Stochastic generation of annual, monthly and daily climate data: A review, *Hydrol. Earth Syst. Sci. Discus.*, *5*, 653–670.

Stephenson, D., K. R. Kumar, F. Doblas-Reyes, J. Royer, F. Chauvin, and S. Pezzulli (1999), Extreme daily rainfall events and their impact on ensemble forecasts of the Indian monsoon, *Mon. Weather Rev.*, *127*, 1954–1966.
Suhaila, J., K. Ching-Yee, Y. Fadhilah, and F. Hui-Mean (2011), Introducing the mixed distribution in fitting rainfall data, *Open J. Mod. Hydrol.*, *1*, 11–22.
Thayyen, R. J., A. Dimri, P. Kumar, and G. Agnihotri (2013), Study of cloudburst and flash floods around Leh, India, during August 4–6, 2010, *Nat. Hazards*, *65*, 2175–2204.
Thiede, R. C., and T. A. Ehlers (2013), Large spatial and temporal variations in Himalayan denudation, *Earth Planet. Sci. Lett.*, *371*, 278–293.
Tucker, G. E. (2004), Drainage basin sensitivity to tectonic and climatic forcing: Implications of a stochastic model for the role of entrainment and erosion thresholds, *Earth Surf. Processes Landforms*, *29*, 185–205.
Tucker, G. E., and R. L. Bras (2000), A stochastic approach to modeling the role of rainfall variability in drainage basin evolution, *Water Resour. Res.*, *36*, 1953–1964.
Tucker, G. E., and R. Slingerland (1997), Drainage basin responses to climate change, *Water Resour. Res.*, *33*, 2031–2047.
Wang, B. (2002), Rainy season of the Asian-Pacific summer monsoon, *J. Clim.*, *15*, 386–398.
Whipple, K. X. (2004), Bedrock rivers and the geomorphology of active orogens, *Earth Planet. Sci.*, *32*, 151–185.
Wolman, G. M., and J. P. Miller (1960), Magnitude and frequency of forces in geomorphic processes, *J. Geol.*, *68*, 54–74.
Wulf, H., B. Bookhagen, and D. Scherler (2010), Seasonal precipitation gradients and their impact on fluvial sediment flux in the Northwest Himalaya, *Geomorphology*, *118*, 13–21.
Wulf, H., B. Bookhagen, and D. Scherler (2012), Climatic and geologic controls on suspended sediment flux in the Sutlej River Valley, western Himalaya, *Hydrol. Earth Syst. Sci.*, *16*, 2193–2217.
Wulf, H., B. Bookhagen, and D. Scherler (2016), Differentiating between rain, snow, and glacier contributions to river discharge in the western Himalaya using remote-sensing data and distributed hydrological modeling, *Adv. Water Resour.*, *88*, 152–169.
Yatagai, A., K. Kamiguchi, O. Arakawa, A. Hamada, N. Yasutomi, and A. Kitoh (2012), APHRODITE: Constructing a long-term daily gridded precipitation dataset for Asia based on a dense network of rain gauges, *Bull. Am. Meteorol. Soc.*, *93*, 1401–1415.
Zhisheng, A., J. E. Kutzbach, W. L. Prell, and S. C. Porter (2001), Evolution of Asian monsoons and phased uplift of the Himalaya–Tibetan plateau since late Miocene times, *Nature*, *411*, 62–66.